XX Polish Fluid Mechanics Conference,
Gliwice, 17-20 September 2012

A NUMERICAL STUDY OF FREQUENCY AND AMPLITUDE EFFECTS IN FLOW AROUND AN OSCILLATING NACA AIRFOIL

Maciej M. Karczewski
Technical University of Lodz, Institute of Turbomachinery, Lodz, Poland
E-mail: maciej.karczewski@p.lodz.pl

Abstract

Accurate prediction of airfoil performance metrics (lift, drag, and moment coefficients) at the design stage of stationary and rotary wings is vital in order to maximise flight efficiency and also for flight controls and avionics. To date, a large number of papers was published, where oscillating (heaving, pitching) airfoils were studied (see for example Yu et al. 2010, Yang et al. 2004). Majority of this research is conducted at low to moderate Re number, oftentimes with focus on Unmanned Aerial Vehicles (UAVs) or Micro-Air-Vehicles (MAVs), while some applications require understanding of flow around airships experiencing flight in fully turbulent flow (chord based Re numbers > 10^6).

One such area of application is flow over a stabiliser of an airship able to perform a wide range of manoeuvres (i.e. helicopter). In such case, its flight path can lead to fluctuations of lift and drag on the stabiliser. For flight controls, an accurate pitch angle on the stabiliser must be set to maintain trim of the airship. Often, at the design stage, it is assumed that the lift vs. angle of attack and drag vs. angle of attack characteristics of an airfoil are going to be linear during flight, while, in reality, oscillations lead to hysteresis.

At the Institute of Turbomachinery a numerical study of pitching oscillation was performed for a NACA 0016 profile, where oscillation frequency, amplitude and initial angle of attack were varied. Alongside, several tests, including dynamic mesh deformation, were made to establish an appropriate methodology to study such phenomena.

Key words: oscillating airfoil, pitching airfoil, Computational Fluid Dynamics (CFD)

NOMENCLATURE

a	sound velocity
c	airfoil chord
c_d, C_d	coefficient of drag
c_l, C_l	coefficient of lift
c_m, C_m	coefficient of moment
F	force
f	frequency of forced motion
i, j, k	body-fitted coordinate system
k	reduced frequency ($2\pi fc/2V$)
l	airfoil thickness
M	moment
Ma	Mach number
Re	Reynolds number
t	time
T	time period
V	freestream velocity
x, y, z	Cartesian coordinates
y^+	non-dimensional wall distance

Greek Letters

α	angle of attack
α_i	initial angle of attack
$\Delta\alpha$	amplitude of pitch
ν	kinematic viscosity
ρ	air density at ISA = 0 m
φ	phase angle
ω	angular frequency ($2\pi f$)

Subscripts

$c/4$	quarter chord
d, D	drag
l, L	lift
m, M	moment

Abbreviations

AoA	Angle of Attack
FFT	Fast Fourier Transform
ISA	International Standard Atmosphere

INTRODUCTION

The specifics of oscillations at high Re number are of vital importance for prediction of a dynamic stall of a helicopter blade. A helicopter main rotor experiences a wide range of velocities along its blade from moderately low near the hub to Mach 0.9 at the tip. This profound difference results in imbalance of lift between advancing and retreating blade. To minimise the effects of this imbalance and avoid dynamic stall, cyclic pitching of blade is introduced.

Therefore, airfoil pitching, a building block of rotary wings, was studied extensively by many teams worldwide in order to control the dynamic stall. For example (McCroskey, 1972) categorised the type of dynamic stall onset types, (Carr, McAllister, & McCroskey, 1977) studied the effect of several parameters on the stall behaviour, reporting that reduced frequency and amplitude of oscillations have the most profound effect. Most recently, (Yu, Hu, & Wang, 2010) found similar results but at lower Ma numbers and performed extensive numerical testing of pitching oscillations. (Young & Lai, 2004) also arrived at similar conclusions. Additionally, recent development in PIV measurement techniques resulted in detailed studies of flowfield patterns experimentally. (Wernert, Koerber, Wietrich, Raffel, & Kompenhans, 1997) showed advantages of this technique over LDA and concluded that vortex shedding in airfoil's oscillatory motion is non-reproducible at some reduced frequencies. (Scholz & Kaehler, 2006) use the PIV to validate their numerical code. However, the study of pitching of airfoils for helicopter rotor dynamic stall prediction is not the only area of interest.

The study presented herein gives an insight on an aerodynamic impact of wing pitching on performance of a helicopter's horizontal stabiliser. The objective was to observe the influence of the forced oscillations of AoA on the aerodynamic performance coefficients (lift, drag, and moment) of the NACA 0016 airfoil.

Explored were the following parameters:

- initial angle of attack (α_i)
- amplitude of oscillation ($\Delta\alpha$)
- reduced frequency of oscillation ($k=\frac{\pi f c}{V}$)

related by the following equations:

$$\alpha = \alpha_i - \Delta\alpha \cdot \cos(2\pi f t) \qquad \text{Eq. 1}$$

$$\frac{d\alpha}{dt} = \Delta\alpha \cdot 2\pi f \cdot \sin(2\pi f t) \qquad \text{Eq. 2}$$

The work was divided into two parts – computing a steady-state flow past the airfoil for a number of angles of attack (1), and time-accurate flow simulations with forced oscillations of the airfoil (2). The following specifications were stated:

1) Static polar: ($\Delta\alpha = 0°$)
   sweep on α : 0°, 5°, 10°, 15°, 17.5°, 20°, 22.5°, 25°

2) Time-dependent dynamic polar:

a)	b)	c)
$\alpha_i = 5°$	$\alpha_i = 5°$	$\alpha_i = 10°$
$\Delta\alpha = 1°$	$\Delta\alpha = 0.2°, 0.5°, 1°, 2°$	$\Delta\alpha = 1°$
k = 0.05, 0.14, 0.27, 0.41, 0.55, 0.68	k = 0.14	k = 0.05, 0.14, 0.27, 0.41, 0.55, 0.68

Ma = 0.33 and chord-based Re = 7.13×10^6 in each case.

The influence of each parameter on the airfoil's aerodynamic characteristics was established along with the type of hysteresis between aerodynamic coefficients and α during forced airfoil oscillations. The reason for this was to validate the engineering design approach for assessing the performance of the horizontal stabilizer. Such high Re number is not usually

tested in wind tunnels, hence limited availability of experimental data for verification of numerical study is a concern. The numerical model is first verified against experimental data gathered in (Sheldahl & Klimas, 1981) for an airfoil NACA 0015. Some results presented are next verified against measurements performed for NACA 0012 airfoil by (Halfman, 1948). Finally, conclusions are drawn in order to assess the influence of aforementioned parameters onto the behaviour of lift, drag, and moment against the angle of attack.

NUMERICAL MODEL

In order to increase computational fidelity and assure a relative independence of results, dozens of tests were run in which a number of mesh and simulation control parameters were varied, for example:

- differing mesh density around the NACA 0016 airfoil,
- moving the mesh boundaries further away from the model to check the influence of the boundary condition proximity on the lift generation,
- utilizing different turbulence models and the modeling of the laminar-turbulent transition,
- verifying mesh periodicity topology;
- for time accurate computations, inspecting various time step values.

The tests also allowed to identify an optimal mesh size to computational time ratio. All but the last trials were launched only for the airfoil inclined at $\alpha = 10°$, where it generated a non-symmetrical flow patterns. The time step for transient analysis was checked for each tested angle. Each time, the results were compared to one another and to an available outside data in order to tune the numerical model.

Experimental wind tunnel data

The data from wind tunnel tests performed for the flow past the NACA 0016 airfoil is not abundant and not easily accessible as such profile is not, contrary to standard NACA 0012, a popular airfoil to research. This limitation required the calculations to be also compared, at least qualitatively, to the experiment performed for a NACA 0015 airfoil that most closely resembles the NACA 0016. Tests run at two Re numbers $Re = 5\times10^6$ and $Re = 10^7$(Sheldahl & Klimas, 1981) were selected as reference.

Domain and mesh sizes

The computational domain was divided into two sections – larger Outer domain and a smaller Inner domain. This selection was not arbitrary – it simplified modeling of the airfoil oscillations in the second stage of the project. Fig. 1 below presents this concept graphically.

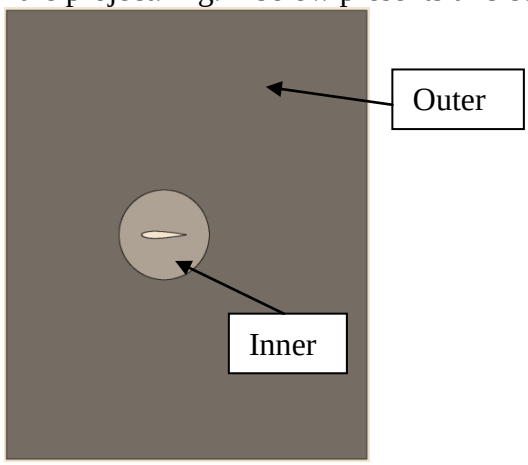

Fig. 3.1. Outer and Inner domains of the computational space

The size of the Outer computational domain was varied to ensure that recorded lift, drag, and moment values would be relatively free of error coming from the imposed boundary conditions. Three domain sizes were compared. The size of the mesh inside the Inner domain were kept identical in each case.

The entire grid was built from structured hexahedral elements with only 2 nodes in *z*-direction (*k* index) and a varying number of nodes along the *x*- and *y*-axis (*i* and *j* indices respectively). Therefore, all computations were run as quasi 3-dimensional. Three combinations of nodal distributions for Inner domain were checked:

a) $i = 550$ $j = 39$
b) $i = 600$ $j = 40$
c) $i = 780$ $j = 60$

From case a) to c), the amount of computational nodes gradually increases. This produces finer grids, thereby enhancing the fidelity of results, but at the expense of computational time. For the mesh around the airfoil wall, the first cell size was kept small enough to ensure maximum y+ values around 2 for all grids in order to use the ω-based equation to compute boundary layer flow. Figure 2 presents the mesh around the airfoil.

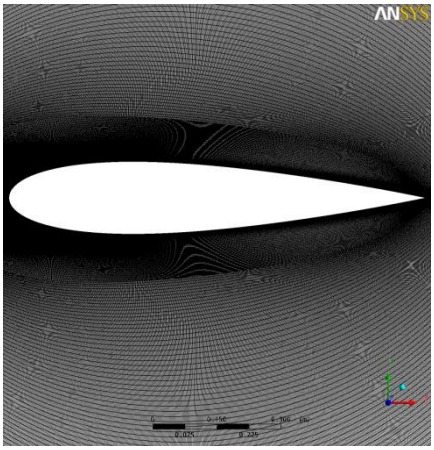

Fig. 2. The structured mesh around the NACA 0016 airfoil

Tab. 1. Compilation of various mesh studies for NACA 0016 CFD simulation. Lift coefficients for $\alpha = 10°$ are compared (note the Re number differences)

Tested meshes	NACA0016 $Re=7.13\times10^6$ CFD	NACA0015 $Re=5\times10^6$ Exp.	NACA0015 $Re=10^7$ Exp.
550×39×1 Speziale/Sarkar/Gatski (SSG)	0.919	1.069	1.100
550×39×1 Shear Stress Transport (SST)	0.919		
600×40×1 SST	0.921		
780×60×1 SST	0.922		
550×39×1 SST+transition model γ-θ	0.929		
550×39×1 SST+transition model γ-θ B1	0.999		
550×39×1 SST+transition model γ-θ B2	1.039		
550×39×1 SST+transition model γ-θ B3	1.079		

For the study airfoil walls were treated as smooth, non-slip and adiabatic. Top and bottom sides of the domain were made periodic translation-wise, while domain sides (facing the reader in Figure 1) had symmetry boundary condition. The interface between Inner and Outer sections was treated as a general connection (hanging nodes on both sides were allowed).

Numerical model independence study

Table 1 presents the compilation of results for some of the tested meshes. Compared are the lift coefficients for the airfoil inclined at $\alpha = 10°$. The final mesh selected for computations is the last one. It falls with its lift coefficient between the two reference NACA 0015 experiments done at Re numbers of the required magnitude.

Two turbulence models were tested - one based on Reynolds Stresses (SSG) and one using two equation model for turbulence closure (SST). As practically, no variation was discovered the latter was chosen for further testing. Varying mesh size had also little impact on the lift coefficient value but increased the computational time. The size 550×39×1 (over 21000 in-plane nodes) guaranteed satisfactory independence what is in general agreement with findings of (Yu, Hu, & Wang, 2010) where independence was reached at 347×47×1 (16000 in-plane nodes).

A visible improvement was reached by introduction of laminar-turbulent transition model. As experiments, for example, by (Wernert, Koerber, Wietrich, Raffel, & Kompenhans, 1997) showed, during airfoil oscillations flow is expected to transition from a laminar separation bubble, near the airfoil leading edge, to fully turbulent boundary layer thereafter. The domain sizing (B1, B2, B3) helped to increase fidelity of the model by minimising impact of location of the imposed boundary conditions.

STATIC POLAR COMPUTATIONS

Simulations were run on a number of workstations each equipped with 4 64-bit Pentium Xeon Dual Core processors and 32 GB of memory. The CFD Solver used was ANSYS v. 12.0 installed on Suse Linux Enterprise Server 9.3 and Windows Vista operating systems both in a 64-bit software versions. The computations were fully implicit second order accurate in time and space. For turbulence closure SST turbulence model was selected. Two equation γ-θ model by Langtry-Menter (ANSYS, 2012) was used for the simulation of the laminar-turbulent transition.

Figure 3 presents the lift and drag coefficient results of the static polar for NACA 0016 simulation. These are compared to the aforementioned NACA 0015 polar treated as reference.

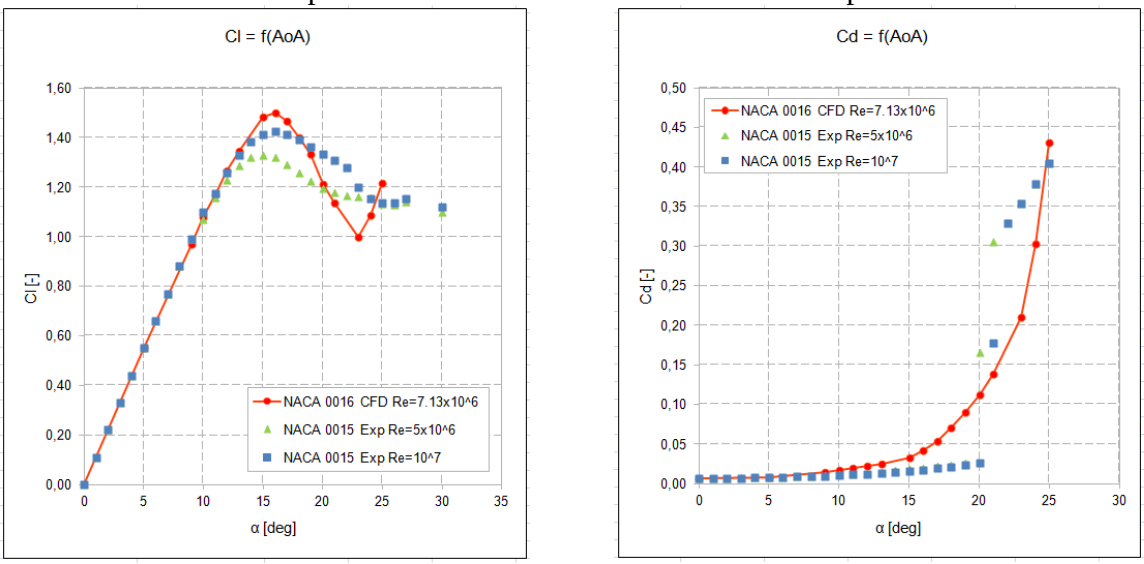

Fig. 3. Lift and drag coefficients - validation of the numerical model

Results show that the model is able to predict the lift and drag values correctly for a wide range of AoA's up to about 13 degrees. This is desired as the maximum AoA for airfoil oscillations will reach 11 degrees. The model correctly predicts the angle for which the static stall occurs, but falls short to predict lift and drag curves beyond that point. This is a known deficiency of many RANS turbulence models. Please note that, although very similar, two different airfoil geometries are being compared hence slightly higher maximum value for NACA 0016 is observed.

MOTION STUDY

Numerical models of oscillation

In order to develop a reliable numerical model of the oscillations, several methods of moving the mesh have been analyzed. They are presented in the pages to follow.

Rotating Domain (RD) – the airfoil and Inner computational domain that encloses the model both oscillate (rotate sinusoidally) in respect to larger stationary Outer computational domain (see Figure 4). Three variations were proposed within it.

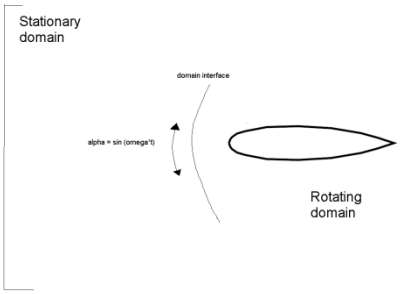

Fig. 4. Rotating Domain (RD) model of oscillation

In the first one, the interface between Outer and Inner domain was chosen to be Frozen Rotor. By doing so the frame of reference and pitch was changed but the relative orientation of the Inner and Outer subdomains across the interface was fixed. The two frames of reference connect in such a way that they each have a fixed relative position throughout the calculation. If the frame changes the appropriate equation transformations are made. If the pitch changes, the fluxes are scaled by the pitch change. This method is labeled as FR on the graphs to follow.

The second variation uses the Transient Rotor Stator interface model. This fully reproduces the movement on the interface boundary. Within this method, two options were verified.

Initially, the advection terms in the Navier-Stokes momentum equation were computed in respect to the relative frame velocity. These results are going to be labeled as TRS. Such approach, however, produced incorrect results, when compared to available experimental data. Therefore, an alternate rotation model was applied in which the advection was now modeled by taking the absolute frame velocity into account. In effect, the amplitude unsteadiness was smoothed out. This method is named as TRSaltRM.

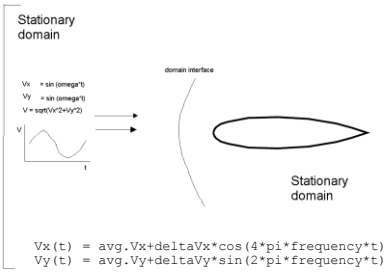

Fig. 5. Oscillating Boundary Conditions (osc. BCs) model

Oscillating Boundary Conditions (osc. BCs) was another model tried. In this case, both computational domains are stationary. Instead, the inlet velocity V is oscillated (actually its components V_x and V_y - see Figure 5). That way the airfoil actually "sees" ambient conditions as oscillating around it. However, this approach was not computationally stable for one of the two cases tested and was neglected as less promising.

Mesh Motion (MM) – in this approach both computational domains are also stationary, but this time the airfoil and the mesh around the airfoil (see Figure 6) are forced to oscillate. The mesh further away is constrained (displacement is diffused, or sequentially diminished with increasing distance away from the airfoil wall). This method is possible for small amplitudes of motion and requires very small time step for simulations.

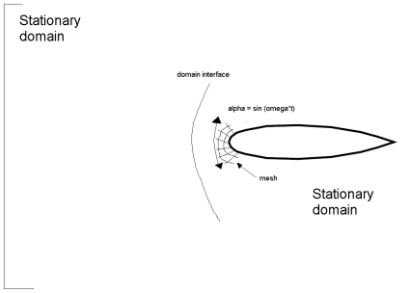

Fig. 6. Mesh Motion (MM) model of oscillation

Consequently, the 3D numerical solution is obtained at a penalty of time, but its level of fidelity is likely to be higher than that offered by the RD and osc. BCs models. The MM method was therefore selected as the one to which other models were compared. The next section, presenting an experiment on oscillating foils done by NACA, confirms that this assumption was valid.

Figure 7 presents the comparison between the numerical motion methods on the basis of time-dependent lift coefficient values computed for $\alpha = 5°$, $\Delta\alpha = 1°$, $k = 0.68$ case. For clarity the angular position of the airfoil is also presented.

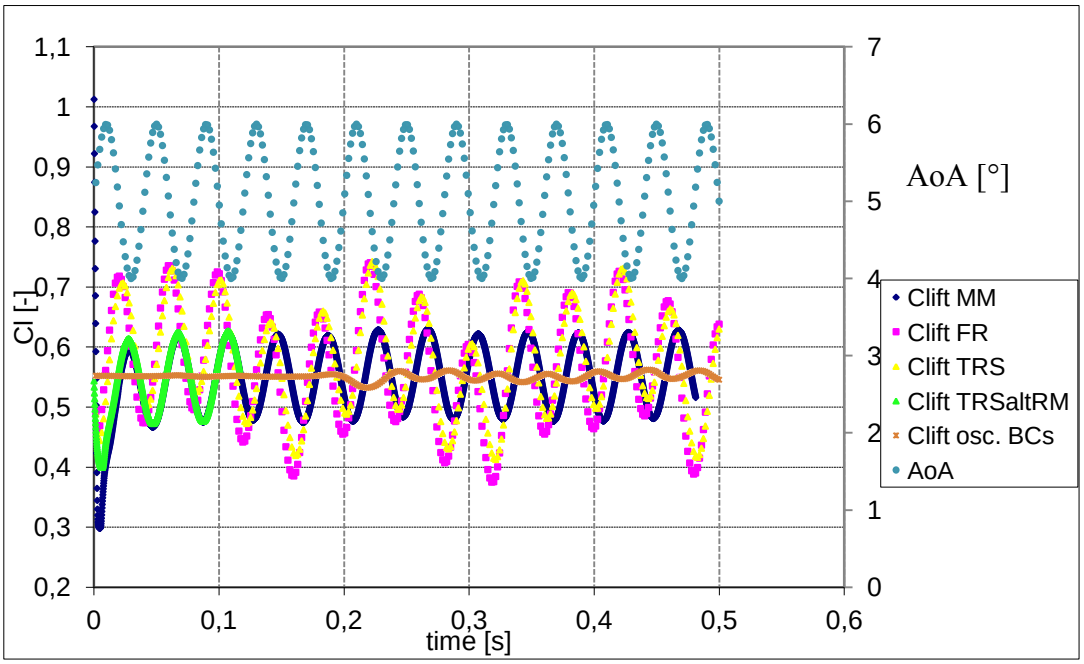

Fig. 7. Time history of lift coefficient for 5 of the model rotation methods

The yellow TRS and pink FR curves give nearly identical results, when compared to one another. However they are not in sync with the MM approach. The difference is in lift amplitude and also in phase angle φ when compared to the angular position of the airfoil at every instant of time (light blue curve). Namely, the curve obtained by FR/TRS method leads the curve obtained by MM method.

The osc. BCs procedure, on the other hand, does not compute the lift amplitudes correctly. It takes about 0.2 s for the oscillations to develop. This is how much time the oscillated air needs to travel from the Inlet boundary to the airfoil's leading edge. Hence a solid non-oscillated orange part is seen in the mentioned time interval.

Finally, only one other approach (TRSaltRM) produced identical results as the MM, but at a fraction of computational time, despite the fact that time step value was equal in both cases. Therefore, the alternate rotation model TRSaltRM method was chosen for further studies.

In order to determine the correct response of aerodynamic coefficients to forced oscillations, a NACA experiment is presented. It was performed on NACA 0012 airfoil in the 1948 (Halfman, 1948). Figure 8 shows the time history of the lift, drag and moment coefficients. The angular position of the airfoil is also plotted. In this work the average angle α_i = 6.1°, whereas amplitude of oscillations $\Delta\alpha$ = 6.7°, so much larger than in the studied NACA 0016 case. The experiment was performed quite some time ago and hence:

- it is necessary to mention that resistance wire strain gages mounted on the cantilevers (they oscillated the airfoil in this experiment), measured the forces required to oscillate the airfoil in a given motion;
- the inertia reactions were subtracted from the signal recorded and, therefore, the functions seen on the plot in Figure 8 are due to pure aerodynamic forces;
- the signals were amplified and recorded with Consolidated Engineering Corporation 1000 cycle-per-second carrier equipment;
- for calibration a reference-position signal was at first obtained from an undamped accelerometer and also from a Kollsman rotatable transformer.

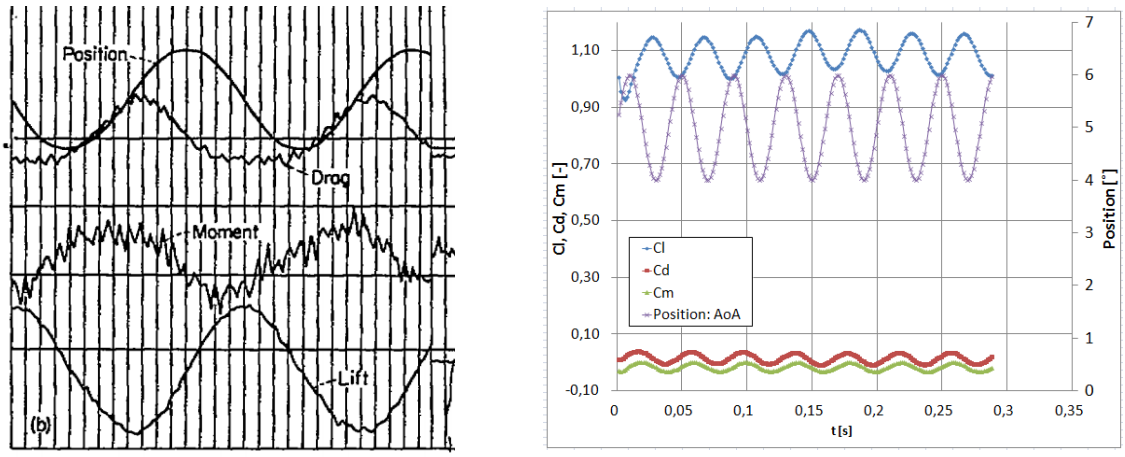

Fig. 8. Time signals of lift, drag, and moment from experiment by (Halfman, 1948) for NACA 0012 as compared to time-accurate predictions from CFD simulation (NACA 0016)

The values of all parameters are not visible, but oscillations of the lift, drag, and moment have forms of sine-like functions, without any amplitude-wise shifts. Particularly, the lift function lags (in phase angle φ) the time position of the airfoil, for each maximum of lift the airfoils exhibits a maximum in drag and moment, what is all reproduced in CFD simulation.

Taking the above into account, CFD computations for all 15 dynamic polar cases presented herein (6 frequency variations for α_i = 5°, where $\Delta\alpha$ = 1°; 6 frequency variations for α_i = 10°, where $\Delta\alpha$ = 1°, and 4 delta variations for α = 5°, where k = 0.14) were performed with the TRSaltRM model.

RESULTS AND DISCUSSION

Influence of reduced frequency and amplitude of oscillation

Figure 9 presents the dependence between the frequency of oscillation k (or angular amplitude $\Delta\alpha$) and the maximal amplitude of aerodynamic coefficients obtained from FFT analysis. Extra points plotted on each graph are results acquired from computations performed with a finer time step.

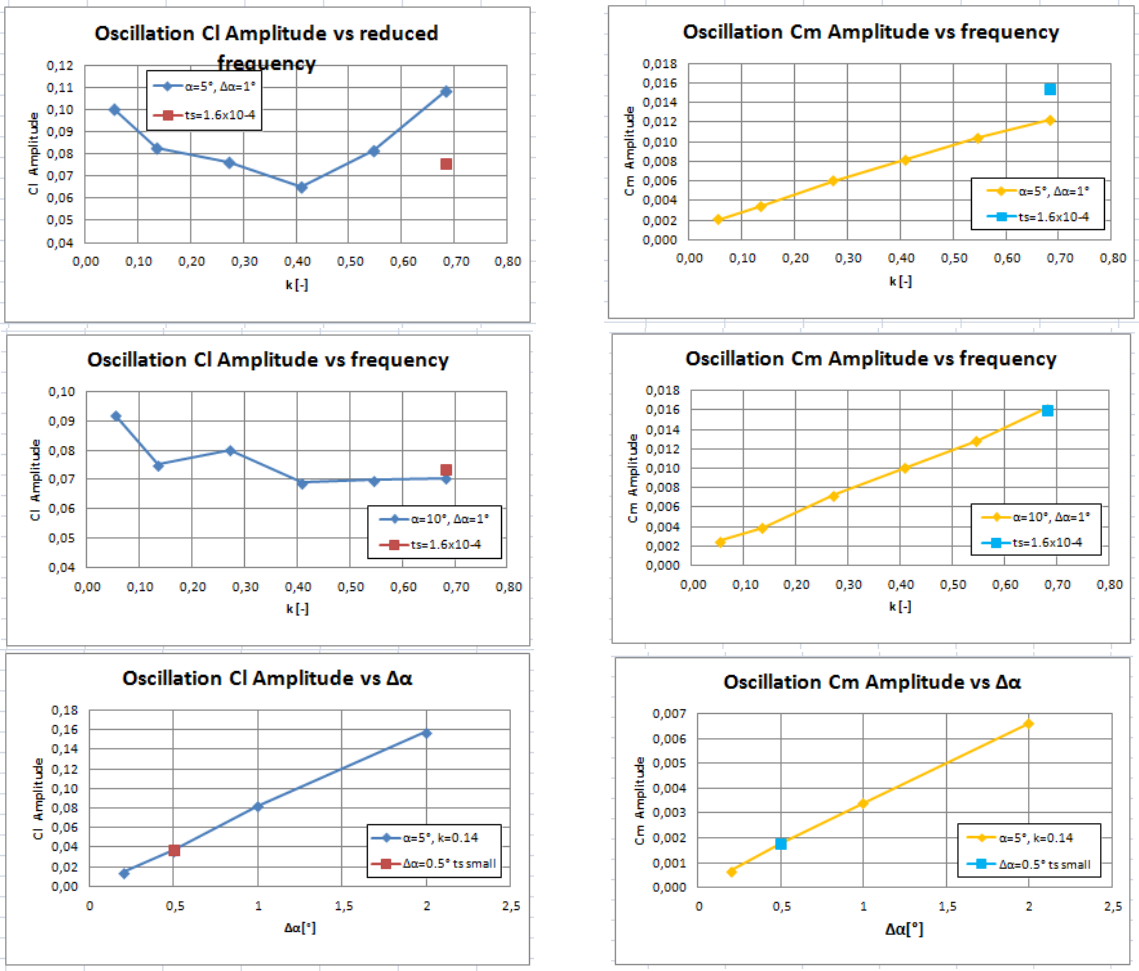

Fig. 9. Relationship between the lift, drag, and moment amplitudes due to forced oscillations and the reduced frequency/angular amplitude for $\alpha_i = 5°$, $\Delta\alpha = 1°$ (first row), $\alpha_i = 10°$, $\Delta\alpha = 1°$ (second row), $\alpha_i = 5°$, $k = 0.14$ (third row)

The plots show that when $\alpha_i = 10°$ and $\Delta\alpha = 1°$:

- the *Cl* values decrease when oscillation frequency increases (finer time step value confirms result at k=0.68),
- pitching moment *Cm* at quarter chord increases linearly with increasing frequencies (finer time step value produced similar results).

Unlike before, when $\alpha_i = 5°$ and $\Delta\alpha = 1°$:

- the *Cl* values first decrease and then increase when reduced frequency increases (finer time step value does not confirm result for $k = 0.68$)
- the *Cm* plot shows similar behavior as when $\alpha_i = 10°$, but the value for k=0.68 with smaller time step seems to be different.

The above discrepancy is attributed to the overestimation of the time step for the computations at smaller AoA's. At $\alpha_i = 5°$, the CFD results obtained from computations with small time step values are rather consistent with the $\alpha_i = 10°$ case. This suggests that similar characteristics are probably to be observed for $\alpha_i = 5°$ as well. The already mentioned

(Halfman, 1948) computed theoretical values of real and imaginary components of oscillating lift signal from the Theodorsen functions and reported that oscillations around an initial angle have exactly the characteristics as presented for the $\alpha_i = 10°$ case studied herein. However, a confirming study would need to be launched for the entire characteristics. Finally, when the amplitude of oscillations increases and the reduced frequency is kept constant ($\alpha_i = 5°$, $\Delta\alpha$ = 0.2°÷2°, k=0.14), the amplitudes of lift, drag, and moment coefficients also rise.

The last section deals with the determination of the type of hysteresis between aerodynamic coefficients and AoA during forced airfoil oscillations.

Hysteresis

Figure 10 presents the results of analysis performed for one of the hysteresis cases.

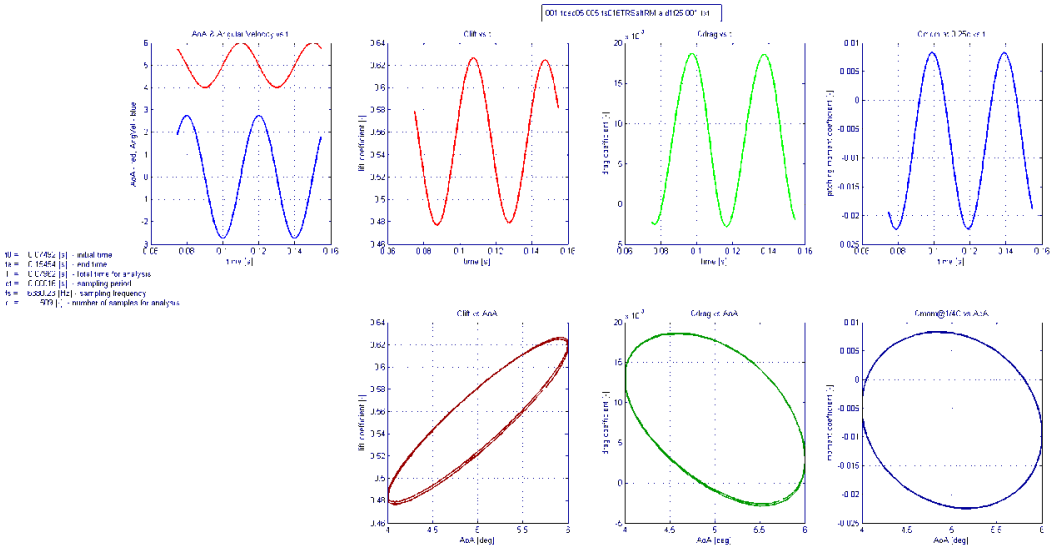

Fig. 10. Time history of lift, drag, and moment for $\alpha_i = 5°$, $\Delta\alpha = 1°$, $k = 0.68$ case along with hysteresis (time step = 0.16×10^{-3} s for CFD simulation), TRSaltRM computation method

The hysteresis suggests that the time-dependent relationships between *Cl*, *Cd*, *Cm* and AoA are non-linear. Figures 11 and 12 along with the discussion offer an overview of the remaining results. There are 2 cases presented:

- case b) where the angular amplitude of oscillations Δα was varied for αi = 5°,
- case c) where the reduced frequency of oscillations k was varied for αi = 10°,
- case a) where k was varied but for a smaller angle, produced similar results as case c).

There are couple of things to be noted from the graphs. Currently, for design purposes, helicopter industry assumes that the in-flight relationship between aerodynamic coefficients is purely linear, where in fact computations show something different. For case b), namely for $\alpha_i = 5°$ the relationship AoA vs. *Cl* is linear, but vs. *Cd*/*Cm* is non-linear.

In cases depicted (2 cycles are presented for all) the hysteresis is the following:

- $\Delta\alpha = 0.2°$, Clift - linear, Cdrag - elliptical, Cmom – quasi-elliptical
- $\Delta\alpha = 0.5°$, Clift - linear, Cdrag –elliptical, Cmom –elliptical
- $\Delta\alpha = 1°$, Clift – quasi-linear, Cdrag – elliptical, Cmom – elliptical
- $\Delta\alpha = 2°$, Clift – quasi-linear, Cdrag – elliptical, Cmom – elliptical

In cases depicted (2 cycles are presented for all) the slopes of coefficients are the following:

- $\Delta\alpha = 0.2°$, Clift - positive, Cdrag - negative, Cmom –negative
- $\Delta\alpha = 0.5°$, Clift - positive, Cdrag - negative, Cmom – negative
- $\Delta\alpha = 1°$, Clift - positive, Cdrag - negative, Cmom – negative
- $\Delta\alpha = 2°$, Clift - positive, Cdrag - negative, Cmom – negative

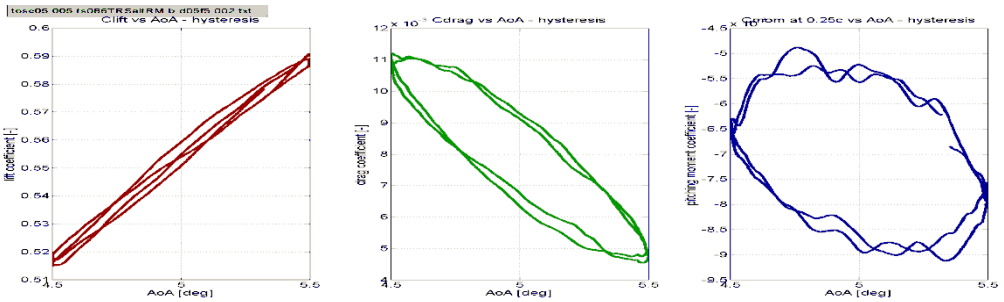

$\alpha = 5°$, $\Delta\alpha = 0.2°$, $k = 0.14$

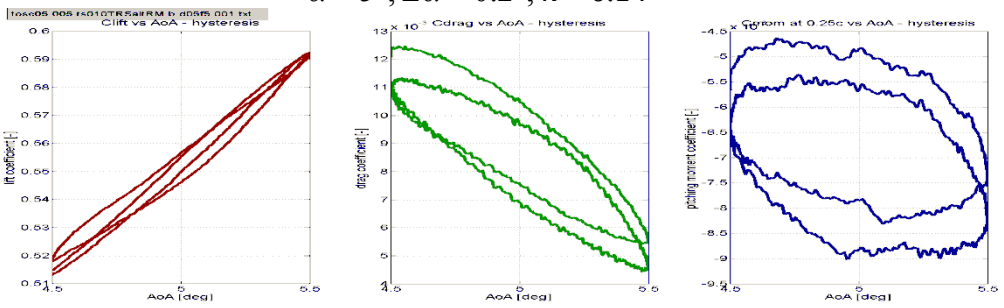

$\alpha = 5°$, $\Delta\alpha = 0.5°$, $k = 0.14$

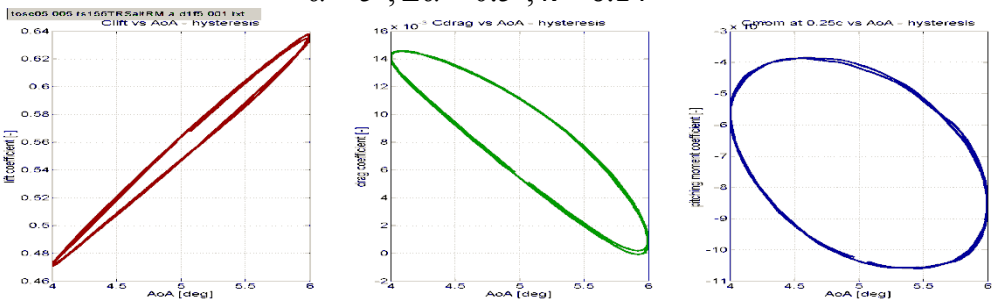

$\alpha = 5°$, $\Delta\alpha = 1.0°$, $k = 0.14$

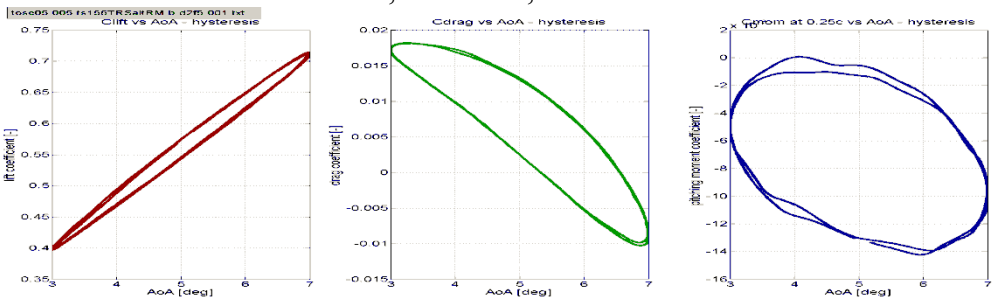

$\alpha = 5°$, $\Delta\alpha = 2.0°$, $k = 0.14$

Fig. 11. Hysteresis information for case b) – delta variation

The amplitude of the oscillations has a significant bearing on the max/min values of *Cl*/*Cd*/*Cm* that are registered for this particular reduced frequency:

- for cases $\Delta\alpha = 0.5°$, $\Delta\alpha = 1°$, $\Delta\alpha = 2°$, the spread between the max/min values of *Cl*/*Cd*/*Cm* increases,
- for cases $\Delta\alpha = 0.2°$, $\Delta\alpha = 0.5$, the spread between the max/min values of *Cl*/*Cd*/*Cm* is nearly identical despite the difference in $\Delta\alpha$.

For case c) (Figure 12) the following can be observed. For $\alpha_i = 10°$, the relationships AoA vs. *Cl*/*Cd*/*Cm* are mostly non-linear. It approaches linear behavior only for the $k = 0.05$ case, but solely for Clift and Cdrag, Cmom remains non-linear. In cases depicted (2 cycles are presented for all) the hysteresis is the following:

- k = 0.05, Clift - linear, Cdrag – quasi-linear, Cmom – elliptical
- k = 0.14, Clift - elliptical, Cdrag - elliptical, Cmom – elliptical
- k = 0.27, Clift – quasi-linear, Cdrag –elliptical, Cmom – elliptical
- k = 0.55, Clift –elliptical, Cdrag – elliptical, Cmom – elliptical

The slopes of coefficients are the following:

- k = 0.05, Clift - positive, Cdrag - negative, Cmom – negative
- k = 0.14, Clift - positive, Cdrag - negative, Cmom – negative
- k = 0.27, Clift - positive, Cdrag - negative, Cmom – negative
- k = 0.55, Clift - positive, Cdrag - negative, Cmom – negative

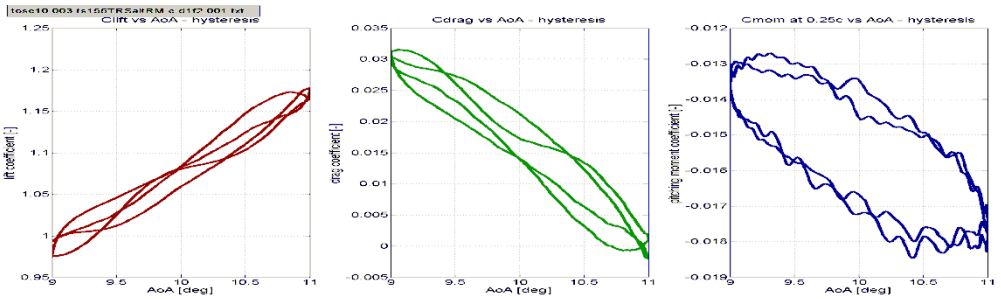

$\alpha = 10°, \Delta\alpha = 1.0°, k = 0.05$

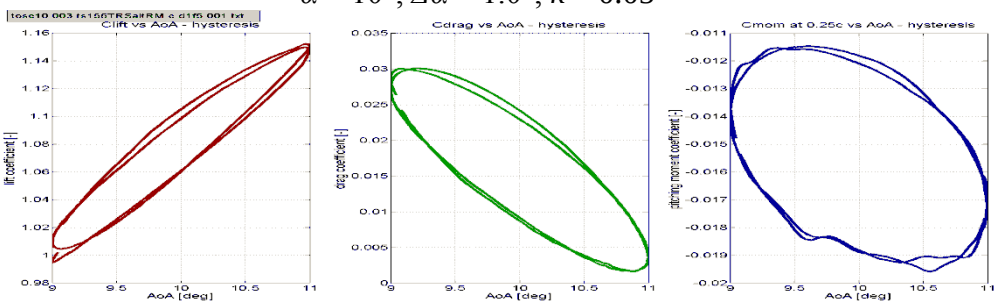

$\alpha = 10°, \Delta\alpha = 1.0°, k = 0.14$

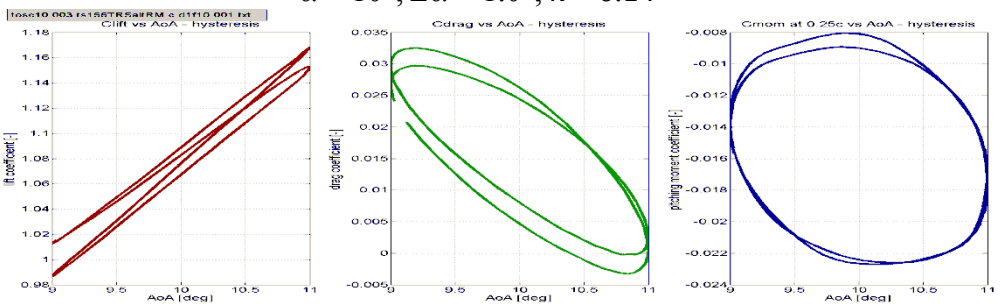

$\alpha = 10°, \Delta\alpha = 1.0°, k = 0.27$

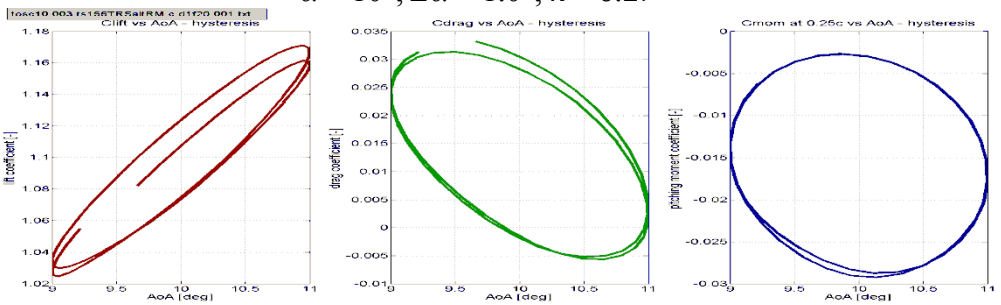

$\alpha = 10°, \Delta\alpha = 1.0°, k = 0.55$

Fig. 12. Hysteresis information for case c) – reduced frequency variation for $\alpha_i = 10°$. 4 out of 5 cases are presented

The frequency of the oscillations has rather insignificant bearing on the max/min values of Clift/Cdrag that are registered for all shown frequencies (this is expected); range of min/max Cmom is more widespread only for higher frequencies.

The results for $\alpha = 10°$ (moderate to high frequencies), remain in good agreement with the data found in numerical study done by NRC (National Research Council) of Canada (Yuan & Schilling, 2002). There, investigated was a NACA0012 airfoil (V = 1 m/s, c = 0.5 m, axis of oscillations at 37% of chord, $\Delta\alpha = 6.74°$, k = 0.31). It seems then that the non-linear relationship between AoA and lift/drag/moment coefficients holds true for low and high flow velocity as well as low and high frequencies.

CONCLUSIONS

Detailed static and time-dependent analysis of NACA 0016 airfoil were performed. The static polar study has revealed a need for verification of the developed numerical model with own experiment as the wind tunnel data for high Re number flow is not available. The search for such kind of information also showed that NACA 0016 airfoil is not a popular wing section to research. On the other hand, the computed lift, drag, and moment values for $\alpha = 5°$ and 10°, two particularly important AoAs for the dynamic polar study, were very consistent with the experimental data used for reference.

The dynamic polar study, where average α_i, reduced frequency of forced oscillations k, and their amplitude $\Delta\alpha$ have been varied, has allowed for a number of important observations. The most important one shows that CFD predicted a grossly non-linear behavior of the hysteresis between AoA and *Cl/Cd/Cm* for nearly all of the studied cases. The current design procedures for horizontal stabiliser of a helicopter assume this relationship to be linear. These findings encourage further investigations of the said phenomenon in order to determine the origin of non-linearity and the frequency and angle values that trigger it.

Above all however, the computations have illustrated that more work on the simulation model itself is still needed. In particular, improvements could be made for computations in case a) (frequency variation for the smaller AoA angle) as well as for lift hysteresis that seems to be inconsistent for one of the cases. Finally, more conclusions could be drawn when a full 3D or even quasi 3D aeroelastic CFD calculations would be launched.

REFERENCES

ANSYS. (2012): ANSYS 14.0 Help: CFX-Solver Theory Guide. *ANSYS CFX Transition Model Formulation*

Carr, L. W., McAllister, K. W., & McCroskey, W. J. (1977): *Analysis of Dynamic Stall Based On Oscillating Airfoils.* Washington, D.C., USA: NASA TN D-8382

Halfman, R. L. (1948): *Experimental Aerodynamic Derivatives of a Sinusoidally Oscillating Airfoil in Two-Dimensional Flow.* Cambridge, MA, USA: NACA TN 1108

McCroskey, W. K. (1972): *Dynamic Stall of Airfoils and Helicopter Rotors.* AGARD 2.1-2.7.

Scholz, U., & Kaehler, C. J. (2006): Dynamics of Flow Structures on Heaving and Pitching Airfoils. *13th International Symposium on Applications of Laser Techniques to Fluid Mechanics.* Lisbon, Portugal, 26-29 June

Sheldahl, R. E., & Klimas, P. C. (1981): *Aerydynamic Characteristics of Seven Symmetrical Airfoil Section Through 180-Degree Angle of Attack for Use in Aerodynamic Analysis of Vertical Axis Wind Turbines.* Albuquerque, NM, USA: Sandia National Laboratories, SAND80-2114

Wernert, P., Koerber, G., Wietrich, F., Raffel, M., & Kompenhans, J. (1997): Demonstration by PIV of Non-Reproducibility of the Flow Field Around an Airfoil Pitchign Under Deep Dynamic Stall Conditions and Consequences Thereof. Paris, France: Gauthier-Villars, *0034-1223*

Young, J., & Lai, J. C. (2004): Oscillating frequency and amplitude effects on the wake of a plunging airfoil. *AIAA Journal , 42* (10), pp. 2042-2052
Yu, M. L., Hu, H., & Wang, Z. J. (2010): A Numerical Study of Vortex-Dominated Flow around an Oscillating Airfoil with High-Order Spectral Difference Method. *48th AIAA Aerospace Sciences Meeting Including the New Horizons Forum and Aerospace Exposition.* Orlando, USA: AIAA Paper 2010-726
Yuan, W., & Schilling, R. (2002): Numerical Simulation of the Draft Tube and Tailwater Flow Interaction. *Journal of Hydraulic Research , 40* (1), 73-81